2008

In-Situ Measurement of Absorption Rates in Horizontal-Tube Falling-Film Ammonia-Water Absorbers: Part I – Measurement Technique

Sangsoo Lee
Samsung Techwin

Lalit Kumar Bohra
Exxon Mobil

Srinivas Garimella
Georgia Institute of Technology

In-situ Measurement of Absorption Rates in Horizontal-Tube Falling-Film Ammonia-Water Absorbers: Part I – Measurement Technique

Sangsoo LEE[1], Lalit Kumar BOHRA[2], Srinivas GARIMELLA[3*]

[1]Samsung Techwin, Power Systems Department
Changwon City, South Korea
Phone : 010-8399-0543 ; E-mail: moonsign@gmail.com

[2]ExxonMobil Upstream Research Company, Gas & Facilities Division
Houston, TX, USA
Phone: (713) 431-7852; Email: lalit.bohra@exxonmobil.com

[3]Georgia Institute of Technology, GWW School of Mechanical Engineering
Atlanta, GA 30332, USA
Phone: (404) 894-7479; E-mail: srinivas.garimella@me.gatech.edu

*Corresponding Author

ABSTRACT

An experimental investigation of heat and mass transfer in a horizontal-tube falling-film ammonia-water absorber was conducted. A tube bank consisting of four columns of six 9.5 mm nominal OD, 0.292 m long tubes was installed in an absorber shell that allowed heat and mass transfer measurements and optical access for flow visualization. This absorber was installed in a test facility consisting of all the components of a functional absorption chiller, which was fabricated to obtain realistic operating conditions at the absorber to account for the influence of the other components in the system. Tests were conducted over a wide range of operating conditions (nominally, desorber solution outlet concentrations of 5 - 40% for three nominal absorber pressures of 150, 345 and 500 kPa, over solution flow rates of 0.019 – 0.034 kg/s.) This paper discusses the development of the test facility, and the measurement and analysis techniques. Results, including the component level heat transfer rates, and solution- and vapor-side heat and mass transfer coefficients, are discussed in the companion paper (Part II).

1. INTRODUCTION

In an absorption heat pump, the absorber, in which refrigerant vapor is absorbed into the dilute solution with the release of a substantial amount of heat of absorption, governs the viability of the entire cycle and has been referred to as the "bottleneck" (Beutler *et al.* 1996). However, a lack of understanding of this inherently complicated process has led to the use of poor designs employing inappropriate and oversized heat and mass exchangers. The ammonia-water fluid pair has a volatile absorbent, thus presenting both heat and mass transfer resistances across the respective temperature and concentration gradients in both the liquid and vapor phases. The highly non-ideal ammonia-water fluid pair releases a considerable amount of heat of absorption at the vapor-liquid interface that must be transferred across a liquid film into the coolant. Absorption is governed by liquid and vapor phase saturation conditions, operating pressures and component geometry. The various driving potentials and local gradients in these phases can be quite different at conditions close to saturation and those that involve subcooling of the incoming liquid solution. The inlet subcooling characteristic of the dilute solution entering an absorber that is part of an operational heat pump system introduces considerable confounding influences that make it challenging to isolate the contribution, to absorption, of the corresponding equilibrium conditions, and those due to the subcooling. The coupled heat and mass transfer processes in both phases have presented challenges for analysis, modeling, experimental validation, and design. In addition, the fluid flow in the respective phases is rarely well defined (as a smooth, laminar film, for example) (Killion and Garimella 2003a). Critical reviews of absorption heat and mass transfer models (Killion and

Garimella 2001) and experiments (Killion and Garimella 2003b) are available in the literature. These reviews have pointed out that research on ammonia-water absorption has often resulted in seemingly conflicting conclusions about the governing transfer resistances, although further analysis could show that the conclusions are not so much conflicting as being limited in the extent of their applicability. Any of a number of transport operations may control the absorption process, with different resistances being dominant in different regions and for different conditions.

In a vast majority of experimental studies, the absorption experiments are conducted on a component test facility that includes only the absorber, solution heat exchanger, and desorber. In such facilities, the dilute solution and vapor are typically generated in a desorber and directly routed to the test absorber at the same pressure and concentration. In an actual absorption system, however, the refrigerant undergoes rectification and expansion to a lower pressure, thus arriving at the absorber at a different concentration and pressure. These conditions are, in turn, influenced by condenser (heat rejection) and evaporation (cooling load) conditions that are determined by ambient and conditioned space conditions. Similarly, the dilute solution undergoes cooling in a recuperative heat exchanger, which leads to a subcooled solution condition at the absorber inlet. Also, these experiments were conducted over a limited range of operating conditions. Therefore, the results from these studies could be valid in their range of test conditions, but not valid for a wide range of operating conditions that apply in complete high efficiency absorption systems over the design range of operation. Many of these studies were conducted at absorber operating pressures in the range 20 - 40 kPa (Jeong *et al.* 1998), 17 - 193 kPa (Kwon and Jeong 2004), and at atmospheric pressures (Haselden and Malaty 1959), whereas the absorber pressure in actual NH_3/H_2O absorption systems for even the refrigeration mode is greater than 150 kPa. Yet other studies were conducted with extremely low vapor concentrations such as 64.7–79.7% (Kang *et al.* 1999) compared to the almost pure ammonia in actual NH_3/H_2O absorption systems. Such studies used very low solution concentrations such as 1.2–2.2% (Jeong *et al.* 1998) at very low pressures (20 – 40 kPa), whereas such low concentrations are rarely seen in absorption systems except at GAX conditions that must also exhibit simultaneously high pressures. Absorber pressures in actual NH_3/H_2O absorption systems are typically between 150–500 kPa for refrigerating, cooling, and heating mode operation. Falling-film studies with or without absorption were conducted with fluids pairs other than ammonia-water, e.g., LiBr/Water (Dorokhov and Bochagov 1983), Water/Glycol (Wilke 1962; Hu and Jacobi 1996a, b), and Water/Oxygen (Nosoko *et al.* 2002). Analytical or numerical studies of absorption phenomena have seldom agreed upon the dominant heat and mass transfer resistances. The liquid-phase mass transfer resistance is considered dominant in some studies (Perez-Blanco 1988; Gommed *et al.* 2001; Fernández-Seara *et al.* 2005; Goel and Goswami 2005), while the others concluded that the vapor-phase mass transfer resistance was dominant (Panchal *et al.* 1997; Potnis *et al.* 1997).

This study investigates heat and mass transfer phenomena in an ammonia-water absorber of a representative geometry operating in a complete absorption system at conditions spanning various modes, i.e., cold ambient and refrigeration (150 kPa), cooling (345 kPa), and warm ambient heating (500 kPa). Experiments are conducted over multiple combinations of solution concentration and absorber pressure for several solution flow rates.

2. EXPERIMENTAL APPROACH

The absorption heat and mass transfer experiments were conducted on a test facility (Figures 1 and 2) replicating a single-stage absorption heat pump. The main components are the absorber, desorber, separator, rectifier, condenser, evaporator, pre-cooler and the solution heat exchanger. The horizontal-tube falling-film absorber assembly (Figure 3) consists of two main parts: an outer shell and a tube array. The absorber tube array is housed in a 0.5 m long × 0.30 m diameter outer shell with a large 0.27 m port, and three additional 64 mm sight ports for illumination and viewing at other angles. The tube array inside the shell consists of four columns of 9.5 mm OD, 0.7 mm wall thickness, 0.29 m long tubes, each column containing 6 tubes, for a total of 24 tubes in the bundle. The tubes are arranged in a serpentine configuration with a horizontal pitch of 30 mm, a vertical pitch of 20 mm, and a surface area of 0.210 m^2. The two absorber coolant headers at either side of the tube array, which allow serpentine flow configuration for the coolant, are 0.13 m long, 0.12 m wide, and 25 mm in depth. The drip tray is placed above the tube bundles, supported by the headers and designed to distribute dilute solution on the tubes. The tray has 4 rows of 75 holes (on a 30 × 3.8 mm pitch) for the insertion of 1.5 mm OD capillary tubes (a total of 300), which distribute the dilute solution on the first row of the tube bundle. The distributor is located 15.0 mm above the centerline of the first row of tubes. Details of the absorber are summarized in Table 1. A distilled water loop is used to remove the heat of absorption from the absorber, which is eventually transferred to the laboratory chilled water-glycol coolant in a plate heat exchanger with a total heat transfer area of 1.65 m^2. An energy balance at the plate heat exchanger

provides an additional means of verifying the results over and above the energy balance between the ammonia and primary coolant in the absorber.

The system operates at two different nominal pressure levels: high pressure at the condenser, rectifier and desorber, and low pressure at the absorber and evaporator. The different solution concentrations at different absorber pressures are obtained by controlling heat duties and temperatures of the desorber, condenser, rectifier and absorber coupling loops. Concentrated solution from the absorber is pumped to the desorber using a magnetic gear pump. The solution pump provides a maximum flow rate of 1.44×10^{-4} m^3/s at zero pressure difference and can be used at up to 1034 kPa differential pressure. A variable frequency drive is used to operate the solution pump. The desorber is a coiled tube-in-tube heat exchanger and uses steam up to a pressure of 690 kPa as the heat source. A two-phase solution consisting of relatively impure vapor and dilute solution exits the desorber outlet and is separated into liquid and vapor streams in the separator. A level indicator is used to monitor the level in the separator. The dilute solution exiting the separator flows back to the absorber, exchanging heat with the concentrated solution from the absorber in a shell-and-tube solution heat exchanger. The vapor from the separator is passed through an externally cooled rectifier, which consists of a 0.483 m long, 0.114 m OD shell that encloses a helical coil of about 12.7 mm tube diameter, with appropriate fill material in the space between the coil and the shell.

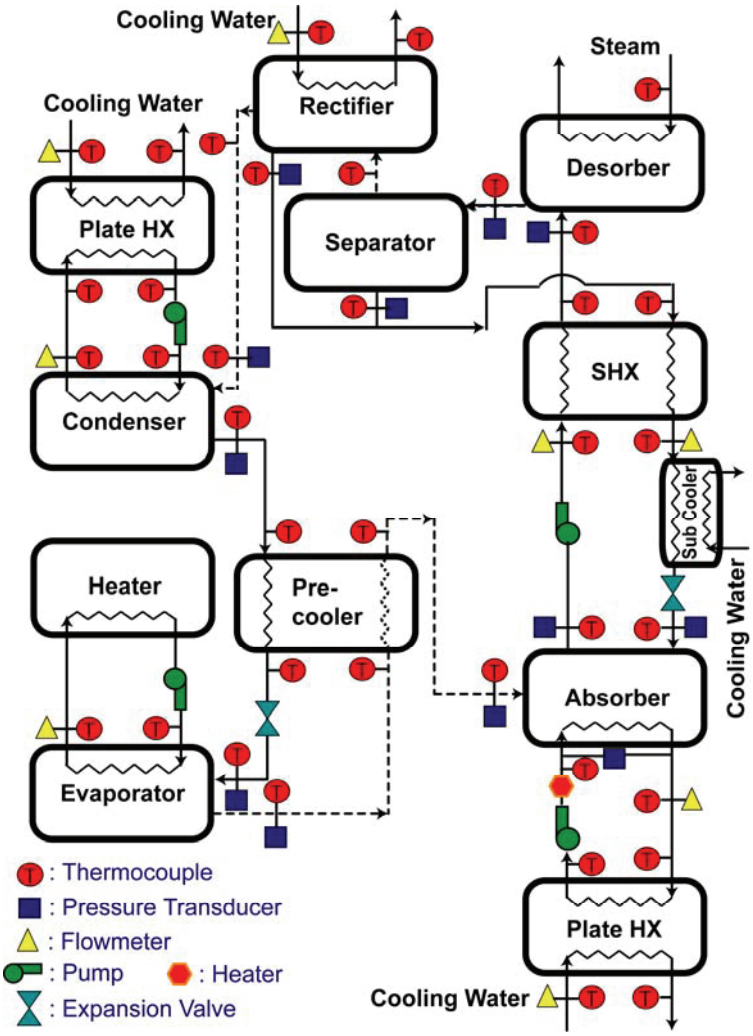

Figure 1. Test Facility Schematic

The ammonia-rich vapor exits the rectifier at the top and flows to the condenser while reflux leaves the rectifier at the bottom and mixes with the dilute solution returning from the separator and flows to the absorber. The rectifier is located at the highest point in the system, thereby providing the necessary pressure difference for the flow of reflux from the rectifier outlet to the separator outlet. A sight glass at the reflux outlet is used to ensure that only liquid reflux leaves the separator from the bottom. The refrigerant vapor is condensed in a shell and tube heat exchanger. Water/glycol solution (nominally 50% by volume) is used as the coolant in the condenser, which in turn exchanges heat with the laboratory chilled water/glycol solution in a plate heat exchanger (identical to one used in the absorber coolant loop). A sight glass at the condenser outlet ensures the liquid state of the condensate. The refrigerant exiting the condenser first flows through a refrigerant pre-cooler, which recuperatively reduces its enthalpy before expansion to the lower pressure. A flow metering needle valve is used as the expansion device. Glycol/water solution (50% by volume) is used as the closed loop heating fluid in the evaporator. A 5 kW electric resistance heater provides the required heating duty to evaporate the refrigerant. Vapor from the evaporator returns to the absorber while exchanging heat with the condensed refrigerant from the condenser in the shell-and-tube pre-cooler heat exchanger. The vapor leaving the pre-cooler is absorbed by the dilute solution in the absorber and the cycle is repeated. A pressure reduction valve is used upstream of the absorber inlet to reduce the high pressure of the dilute

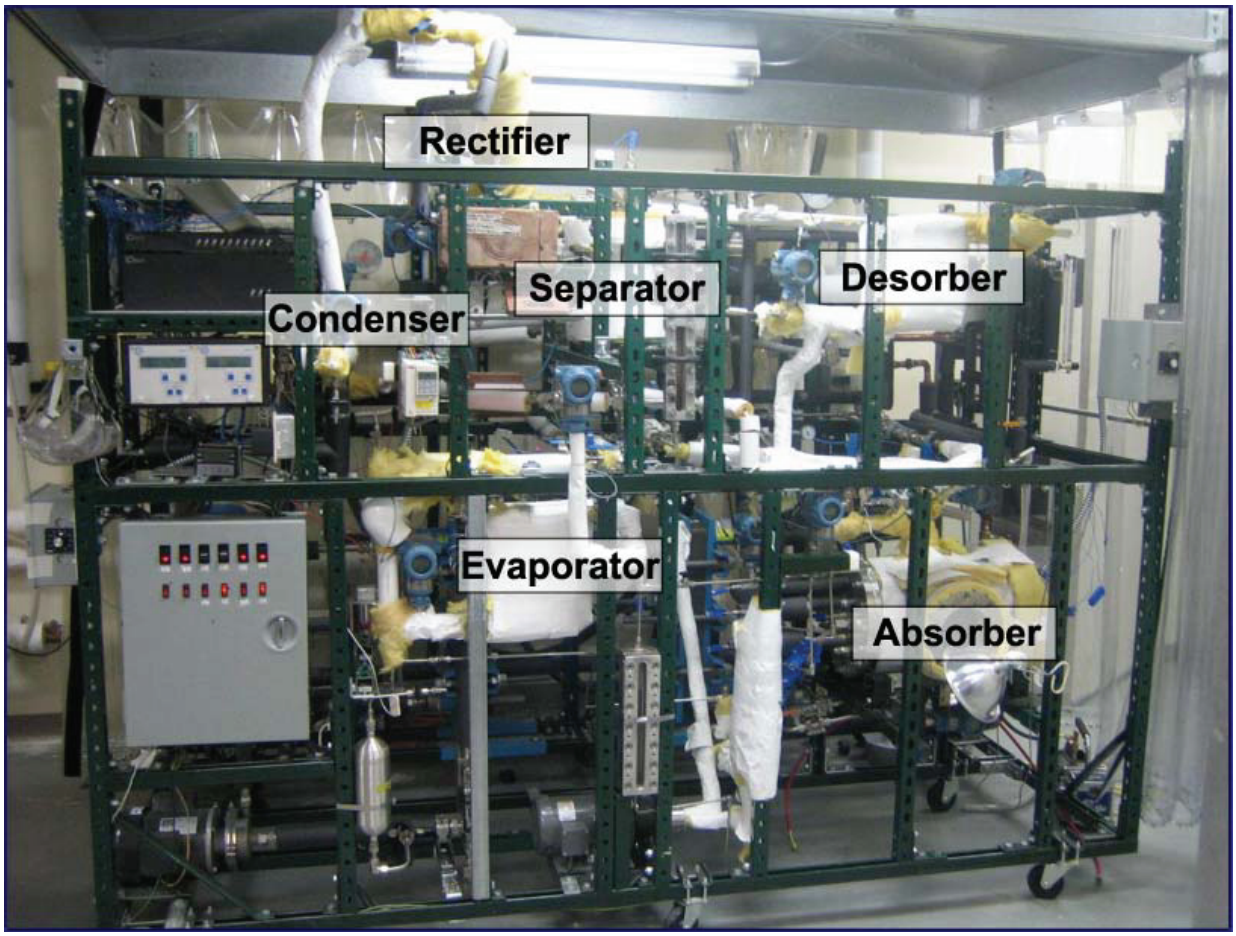

Figure 2. Test Facility Photograph

solution from the solution heat exchanger. For some of the extreme conditions, e.g., low pressure and high dilute solution concentration, this system alone is unable to maintain low absorber pressures of 150 kPa and 345 kPa. To address this issue, an externally cooled sub-cooler is used between the solution heat exchanger and the absorber. This helps reduce the temperature of the dilute solution entering the absorber, therefore reducing the absorber pressure. At the other extreme, e.g., low concentration and high pressure, it is necessary to keep the coolant flow rate very small to maintain a higher absorber pressure. However, this results in unrealistically large coolant temperature differences. To keep the coolant temperature differences reasonable and still maintain the higher absorber pressure, it is necessary to circulate the coolant at higher temperatures. Therefore, a 5 kW electric heater is used in the closed coolant loop to independently control the coolant temperatures. For each pump in the system, an expansion tank is provided upstream of the pump suction port to eliminate the possibility of starving the pump.

Solution-side temperatures at the inlet and the outlet of the condenser, desorber and solution heat exchanger, as well as at the inlet of the pre-cooler and evaporator, are measured using Pr-13 RTDs (Omega) with an accuracy of ±0.5-0.8^{o}C, while the rest are measured using T-type thermocouples (Omega) with an accuracy of ±0.5^{o}C. Absolute solution pressures in the system are measured using Rosemount pressure transducers (models 2088 and 3051) with an accuracy of ±0.25-0.75% of the calibrated span. Dilute and concentrated solution flow rates are measured using Coriolis flow meters (model CMF025 ELITE by Micromotion) with an accuracy of ±0.10% of the flow rate. The refrigerant mass flow rate is measured using a Coriolis flow meter (model D12 by Micromotion) with an accuracy of ±0.10% of the flow rate at the exit of the condenser. The absorber coolant flow rate is measured using a magnetic flow meter (model 8711 by Rosemount) coupled to a flow transmitter (model 8712C by Rosemount), with an accuracy of ±0.5%. The condenser coolant flow rate is measured using a Coriolis flow meter (model CMF100 Elite by Micromotion) with an accuracy of ±0.10%. The flow rate of the coolant in the evaporator loop is measured using a positive displacement flow meter (model JVM-60KL, AW company) with an accuracy of ±0.5% coupled to a flow

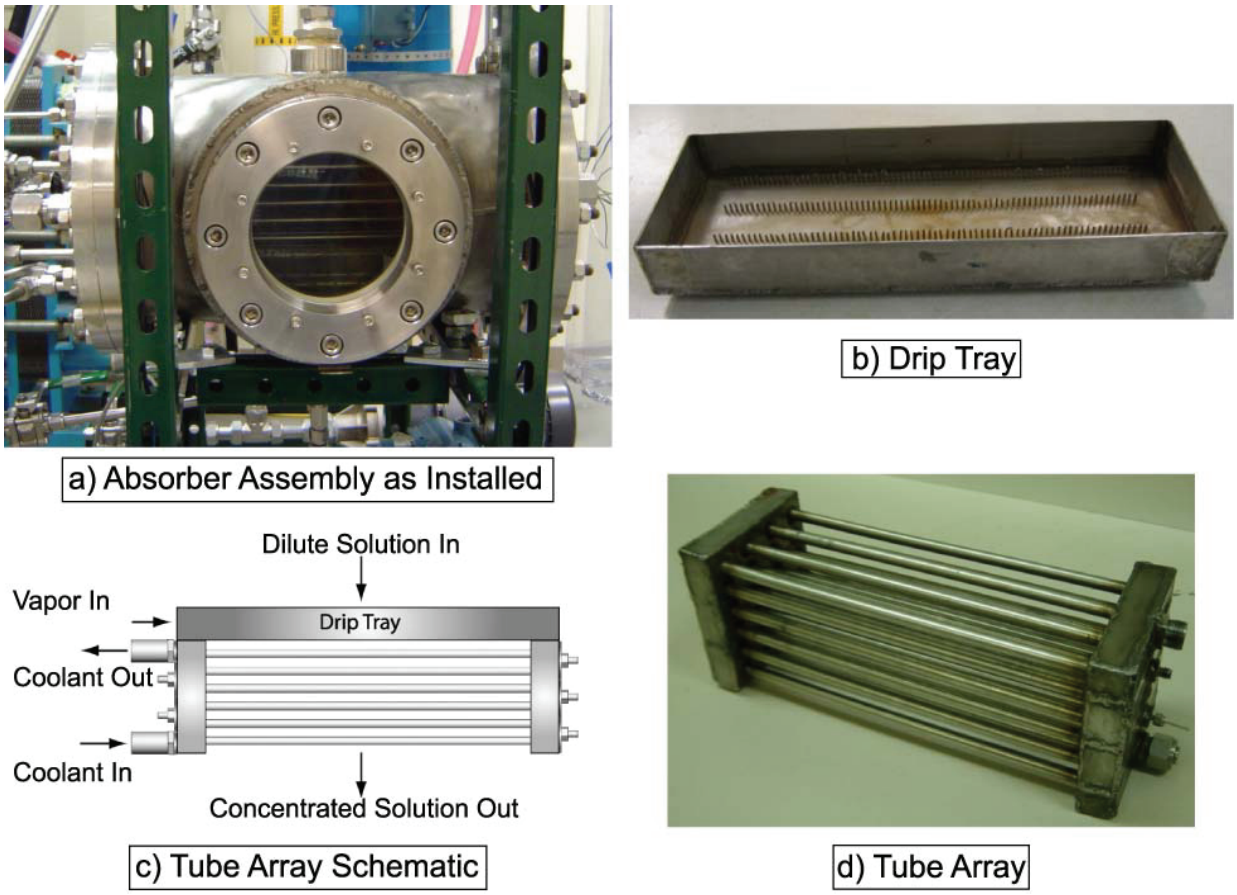

Figure 3. Absorber Geometry

transmitter (FEM-03, AW Company). Other coolant flow rates in the secondary heat exchangers are measured using various rotameters. A PC-based data acquisition system is used to display and record data. Additional details about the test facility and the experimental procedures are available in Lee (2007) and Bohra (2007).

Testing was conducted at nominal absorber pressures of 150, 345 and 500 kPa, with nominal desorber outlet concentrations of 5, 15, 25, and 40%. Also, at each of these combinations of conditions, tests were conducted for three solution flow rates, 0.019, 0.026, and 0.034 kg/s. To obtain data over this wide range of conditions, the laboratory chiller and the steam are adjusted for each data point under consideration. The laboratory chiller has a maximum cooling capacity of 176 kW and provides coolant temperatures as low as -9.45°C. Water-glycol solution from this chiller serves as the heat sink for the rectifier, condenser, and absorber. Laboratory steam lines supply steam at up to 1379 kPa through pressure regulators in the range 0 to 689 kPa and 0 to 2068 kPa. The steam line is directly connected to the desorber and determines desorber outlet temperature and the dilute solution concentration. Once the desired concentration at the desorber outlet, the concentrated solution flow rate, and the absorber pressure are obtained, the system is monitored for steady state. In addition, temperatures were measured at each tube row within the absorber tube array. For each data point, 100 readings were recorded over a duration of 5 minutes, and the average value was used to represent the conditions for that data point.

3. DATA ANALYSIS

3.1 System Level State Points and Properties

The working fluid, which is a binary mixture of ammonia and water, requires three independent parameters to define its state at any location in the system. For each data point, 11 absolute pressures, 1 differential pressure, and 56 temperatures are measured at various locations and used as two of the required independent parameters for directly

establishing the state. For these state points, the additional required parameter is typically either concentration or quality. The quality at any given state was chosen as the third independent parameter (wherever appropriate), because the uncertainties associated with obtaining samples of the vapor and liquid states of the solution at different locations around the test loop during operation are expected to be considerable. At such state points, measured temperatures and pressures, and the expected quality (e.g., saturated liquid or saturated vapor) are used to obtain the solution concentration. Other properties such as enthalpy and specific volume are obtained using these three known independent parameters. (In some instances, the enthalpy obtained from energy balances is used as an input to compute quality or concentration.) The steps to analyze the processes around the test loop are described using a representative data point with the following nominal values: dilute solution concentration at the desorber outlet of 25%, absorber inlet pressure 345 kPa, and a concentrated solution flow rate of 0.026 kg/s.

Table 1. Absorber Geometry

Tube Assembly	
Tube O. D.	9.5 mm
Tube Wall Thickness	0.7 mm
Tube Length	0.292 m
Number of Rows	6
Number of Columns	4
Horizontal Pitch	30.5 mm
Vertical Pitch	20.1 mm
Total Surface Area (A_{Abs})	0.210 m^2
Drip Tray	
Length	0.343 m
Width	0.120 m
Height	38.1 mm
Capillary Tube O. D.	1.5 mm
Number of Rows	4
Capillary tubes per row	75
Pitch (longitudinal)	3.8 mm
Pitch (Transverse)	30.5 mm
Coolant Headers	
Length	0.130 m
Width	0.120 m
Depth	25.4 mm

The ammonia-water solution exits as a two-phase mixture from the desorber, with the liquid and vapor phases in equilibrium with each other. Therefore, the liquid and vapor phase concentrations are computed based on the measured temperature and pressure at the desorber outlet. At desorber outlet conditions of 122.4 ^{o}C and 1110 kPa, the saturated dilute solution concentration is 0.2386, while the vapor exit concentration is 0.8427. The ammonia concentration flowing through the refrigerant circuit of the loop is obtained using an assumption of a saturated vapor condition at the measured rectifier outlet temperature and pressure. The rectifier outlet temperature of 80.99 ^{o}C and pressure of 1127 kPa yield a refrigerant concentration of 0.9781. The reflux concentration is estimated by assuming a saturated liquid state leaving the rectifier at the measured temperature and pressure at reflux outlet location, which, for this representative case with T = 51.4 ^{o}C and p = 1121 kPa, results in x = 0.6182. The vapor concentration at the rectifier inlet is the same as the concentration of the vapor leaving the separator (and therefore, also the desorber). The reflux and rectifier inlet flow rates are calculated using mass and species balances at the rectifier using the refrigerant flow rate, and the concentrations at the rectifier inlet, rectifier vapor outlet and the reflux outlet, to yield a rectifier vapor inlet flow rate of 4.532×10^{-3} kg/s, vapor outlet flow rate of 2.826×10^{-3} kg/s, and a reflux flow rate of 1.706×10^{-3} kg/s. Mass and species balances at the separator outlet are used to find the dilute solution concentration entering the absorber (0.2671), and a species balance at the absorber is used to find the concentrated solution concentration (0.3336). The dilute solution concentration entering the absorber is different from the concentration at the desorber outlet, because the reflux mixes with the solution leaving the separator before it enters the absorber. Once the concentrations were determined, other thermodynamic properties were obtained using *Engineering Equation Solver* (EES) software (Klein 2006) as a function of valid combinations of three independent parameters at various state points in the system.

3.2 Absorber Heat Transfer Calculations

At the absorber, with all the mass flow rates and enthalpies known (from temperature, pressure and concentration), the solution-side heat duty is calculated as follows:

$$Q_{Abs} = \dot{m}_{Dilute} \times h_{Abs,in} + \dot{m}_{Ref,Measured} \times h_{Abs,V,in} - \dot{m}_{Concentrated} \times h_{Abs,out} \quad (1)$$

The resulting solution-side heat duty is 7.854 kW. The coolant-side heat duty, which helps establish the energy balance between the two sides of the absorber, is calculated using the absorber coolant flow rate and temperatures at the inlet and outlet:

$$Q_{Abs,C} = \dot{m}_{Abs,C} \times Cp_{Abs,C} \times \left(T_{Abs,C,out} - T_{Abs,C,in} \right) \quad (2)$$

and yields a duty of 7.954 kW, representing an average heat duty of 7.904 kW, and an error of 1.3%. In the entire data set of 36 points, 20 showed energy balances within 5%, 14 points within 10%, and 2 points within 15%, for an average absolute deviation of 4.77%. Similar calculations were conducted on each of the major components in the system (desorber, condenser, rectifier, evaporator, and solution heat exchanger. These calculations ensured that energy balances were established not just at the absorber, but also throughout the system, which is important because flow rates and concentrations at the absorber, depend to a large extent on system-wide state points.

The overall heat transfer coefficient is obtained from the average absorber duty and the log-mean temperature difference. Initially, a log mean temperature difference (*LMTD*) was defined, along the lines of much of the literature, based on the solution saturation temperatures (corresponding to measured solution pressure, concentration and saturated liquid quality) and the measured coolant temperatures. The *LMTD* based on saturation temperatures represents the idealized driving temperature difference for heat transfer in the absorption process. This *LMTD* definition is preferable when the solution temperature in the absorber is close to its saturation state. However, in the present study conducted on an absorber placed in an actual operating heat pump, the bulk solution is significantly subcooled throughout the absorber. Because the *LMTD* based on saturation temperatures is considerably higher than an *LMTD* based on actual temperatures, it may not correctly represent the heat transfer performance of the absorber. Thus, here, the *LMTD* is defined based on the measured solution and coolant temperatures to calculate the overall heat transfer coefficient in the absorber. For this representative data point, the *LMTD* = 30.87^{o}C, and the resulting overall heat transfer coefficient *UA* is 1221 W/m^2-K. A thermal resistance network consisting of the coolant-side, tube-wall, and solution-side resistances is used to calculate the solution-side heat transfer coefficient. For the representative data point, a coolant velocity of 1.472 m/s yields a *Re* = 13,353. At a Prandtl number of 6.265, using the Churchill (1977b, a) equations, the friction factor and Nusselt number are 0.029 and 104, respectively. The corresponding coolant heat transfer coefficient is 7653 W/m^2-K. With a wall thermal resistance of 5.27×10^{-5} m^2-K/W, the solution heat transfer coefficient is 1632 W/m^2-K. For all the test conditions, it was ensured that the solution-side heat transfer resistance dominates, which minimizes the errors in the estimation of the solution-side heat transfer coefficient from the measured overall heat transfer coefficient.

3.3 Mass Transfer Calculations

In ammonia-water absorption, both refrigerant and absorbent (from the vapor phase) are absorbed by the solution flowing over the tubes, which results in a different concentration of the mass absorbed at the vapor-liquid interface than that of the bulk vapor, with no direct way to measure this concentration. Also, the liquid-vapor interface conditions cannot be measured directly, and some key assumptions are made to determine these conditions. Vapor entering the absorber occupies the vapor space in the large absorber chamber. It is, therefore, not possible to define a preferred vapor flow direction and velocity. In addition, the solution pool at the absorber bottom provides a large solution surface at a relatively constant temperature. It is assumed that the bulk vapor achieves conditions corresponding to saturation at the minimum temperature in the absorber and the average absorber pressure upon entry into the chamber. The minimum temperature in the absorber is the minimum among the absorber outlet, the solution pool and a minimum solution temperature based on a curve-fit of the solution-side thermocouple measurements (solution-side temperatures are also measured at each tube row, in the drip tray and the solution pool). The minimum temperature in most cases was either at the solution pool or at the exit of the tube array. In this case, the minimum temperature was 29.84^{o}C. Based on the average absorption pressure and this temperature, the bulk vapor concentration is established at 0.9965. The absorption process is understood as the progression of the bulk vapor to the interface, and into the bulk solution. During this progression, four distinct regions are identified: vapor sensible cooling or heating region (depending on the interface and bulk conditions) between the vapor bulk and the interface, latent heat region at the interface, the condensed vapor sensible region between the interface and the solution bulk, and finally, the solution sub-cooling region. To compute the mass transfer coefficient and heat duties in these regions, the interface conditions need to be known.

The interface conditions are taken as those of saturation at the solution bulk temperature and absorber pressure. In much of the literature, the interface conditions are assumed to be those corresponding to saturated liquid at the

solution bulk concentration (assuming complete mixing in the solution). However, most of these studies involve saturated solution; therefore, the interface temperature (estimated using the bulk concentration) does not differ significantly from the solution bulk temperature. As discussed above, the solution here is considerably sub-cooled, therefore, assuming the interface liquid concentration to be the same as the solution bulk concentration results in unrealistically high interface temperatures. Therefore, the interface temperature is taken to be equal to the solution bulk temperature. In the representative case, this interface temperature is 50.71°C, with the absorber operating at 351.2 kPa. The corresponding liquid and vapor concentrations at the interface are 0.3716 and 0.9814, respectively. With these temperatures and concentrations now determined, heat duties in each of the absorption regions identified above are computed ($Q_{V,sen}$ = -0.185 kW, Q_{latent} = 3.992 kW, $Q_{cond,sen}$ = -0.071 kW, defined positive for bulk vapor to bulk solution). The resulting solution heat duty is calculated as follows:

$$Q_{soln,sen} = Q_{coolant} - (Q_{V,sen} + Q_{latent} + Q_{cond,sen}) \tag{3}$$

and yields a solution sensible duty of 4.218 kW. As expected, the heat duties of the phase-change at the interface and of the subsequent sub-cooling of the solution are the largest contributors to the overall duty removed by the coolant. The latent heat duty is used for determining the condensing flux concentration as discussed below.

The concentration of the condensing flux (z) is calculated using an energy balance at the interface, equating the latent heat released at the interface to the phase change enthalpies of ammonia and water at the absorber pressure:

$$Q_{Abs,latent} = \dot{m}_{Refg,measured} \times \left(h(T_{int}, P_{int}, q = 1) - h(T_{int}, P_{int}, q = 1) \right) \tag{4}$$

$$Q_{Abs,latent} = z \times h_{fg,NH_3} + (1 - z) \times h_{fg,H_2O} \tag{5}$$

This yields a condensing flux concentration z = 0.8534. It can be seen that the concentration of the vapor mass absorbed at the interface is different from both the bulk vapor and the vapor concentration at the liquid-vapor interface. Preferential condensation of water out of the vapor leads to the lower z = 0.8534 than $x_{v,bulk}$ = 0.9965 and $x_{v,int}$ = 0.9814. This concentration of the condensing flux is used to calculate the mass transfer coefficient (Colburn and Drew 1937) in terms of the molar concentrations:

$$\dot{n}_T = \beta_V \times C_{T,V} \times \left(\frac{\tilde{z} - \tilde{x}_{V,int}}{\tilde{z} - \tilde{x}_{V,bulk}} \right) \tag{6}$$

where $\dot{n}_T$ is the measured molar flux of the vapor absorbed in the solution (a negative sign denotes absorption):

$$\dot{n}_T = \frac{-\dot{m}_{Refg,measured}}{A_{Abs} \times \left(\tilde{z} \times M_{NH_3} + (1 - \tilde{z}) \times M_{H_2O} \right)} \tag{7}$$

The resulting molar flux is -4.721×10^{-4} kmol/m^2-s. The total mass transfer area (0.3487 m^2) in the above equation (different from the heat transfer area) includes the tube array (0.21 m^2), drip tray (0.04 m^2), drops at the capillary tubes (0.01 m^2) and the solution pool (0.09 m^2). The total molar concentration in the absorber (0.1394 kmol/m^3) is obtained using the ideal gas law for ammonia vapor at the average absorber pressure and temperature. These values result in a mass transfer coefficient β_v = 0.030 m/s.

Mass transfer in the liquid-phase is treated primarily as convective mass transfer rather than as diffusive mass transfer as was the case for the vapor phase, since fluid motion in the liquid phase has a more important role. The convective mass transfer in the liquid phase occurs between the bulk liquid solution and the condensing flux that is condensed at the liquid-vapor interface. This convective mass transfer depends on the transport properties and dynamic characteristics of the flowing fluid. The convective mass transfer coefficient is determined as follows:

$$\dot{n}_A = \beta_l \times \Delta C_A \tag{8}$$

where $\dot{n}_A$ is the measured molar mass of species A (ammonia) that is the absorbed into the falling-film, ΔC_A is the difference between the molar concentration at the boundary and the average molar concentration of the bulk fluid stream, and β_l is the convective mass transfer coefficient in the liquid-phase. The above equation can be re-written on a mass basis in terms of the respective mass flow rates and concentrations to yield:

$$\dot{m}_A = \dot{m}_T \times x_{vap,in} = \beta_L \times A_{Abs} \times \left(z_{A,sol,int} \times \rho_{sol,int} - x_{A,sol,bulk} \times \rho_{sol,bulk} \right) \tag{9}$$

which results in $\beta_l = 2.313 \times 10^{-5}$ m/s.

An error propagation method (Taylor and Kuyatt 1994) is used to estimate the uncertainties due to measurements in the parameters of interest. At the representative test condition under discussion, the uncertainties due to the temperature and pressure measurements in the determination of the respective concentrations are: $x_{Abs,in} = 0.2671 \pm 0.0034$, $x_{Abs,out} = 0.3336 \pm 0.0029$ and $x_{Abs,V,in} = 0.9781 \pm 0.0007$. The average absorber heat duty for this case is 7.904±0.48 kW. This average absorber duty and an LMTD of 30.87±0.53°C yield in an overall *U* of 1221±73.97 W/m^2-K. Similarly, the coolant-side heat transfer coefficient is 7653±54.18 W/m^2-K, which yields a solution heat transfer coefficient of 1638±130.9 W/m^2-K. The corresponding mass transfer coefficient uncertainties are 0.0304±0.0018 m/s (vapor) and $2.313\times10^{-5}\pm2.2\times10^{-7}$ m/s (liquid).

Table 2. Absorber Parameters and Uncertainties

Parameter	Range	Uncertainty Range (%)	Average Uncertainty (%)
Q_{Abs} (kW)	3.26 - 10.75	1.30 - 20.50	6.18
U_{Abs} (W/m^2-K)	753 - 1853	2.43 - 15.63	7.95
$\alpha_{Abs,Film}$ (W/m^2-K)	923 - 2857	4.17 - 20.04	11.21
β_V (m/s)	0.0025-0.2541	4.63 - 14.20	7.91
β_l (m/s)	5.51×10^{-6} – 3.31×10^{-5}	0.47 - 2.92	1.06

Absorber heat duties and overall and solution heat transfer coefficients, and vapor- and liquid-phase mass transfer coefficients were obtained using the analyses described above for three different absorber pressures, four different dilute solution concentrations, and three different concentrated solution flow rates. Table 2 shows the ranges of these parameters along with the uncertainties in their calculation.

4. CONCLUSIONS

An experimental investigation of ammonia-water absorption heat and mass transfer in a horizontal-tube falling-film absorber was conducted. The experiments over a wide range of concentration, absorber pressure and solution flow rates cover all postulated absorption system operating modes such as refrigeration, air-conditioning, warm-ambient heat pumping, and cold-ambient heat pumping. Such a study that attempts to understand component level heat and mass transfer in a complete ammonia-water absorption heat pump over realistic operating conditions has not been conducted before. Measured quantities such as temperatures, pressures and flow rates at numerous locations around the test loop were analyzed to obtain absorber heat duties, overall and solution heat transfer coefficients, and mass transfer coefficients in the vapor and liquid phases. Experiments on a complete absorption system introduce three major confounding influences: a) the absorption process itself results from a combination of actual subcooled inlet conditions and the corresponding equilibrium conditions, with the individual contributions difficult to isolate, b) the definition of driving temperature differences becomes a significant issue unlike the situation where the liquid phase enters at near-saturated conditions, c) overall component mass, species and energy balances are affected to a considerable degree by the accuracy with which every other component in the system can be analyzed, whereas in a single-pressure facility, these balances must be accurately established only for the test component, i.e., the absorber. The complete absorption system used in this study could also introduce additional uncertainties in establishing the dilute solution concentration and flow rate entering the absorber, and in the other important flow rates and concentrations, i.e., of the concentrated solution and the ammonia vapor. This is because mass, species and energy balances must be satisfied iteratively and simultaneously in all the major components (desorber, separator, rectifier, condenser, expansion device, refrigerant pre-cooler, evaporator, and absorber, and their respective coupling loops) to be able to obtain the conditions at the absorber. In the present study, the issue of supplying representative inlet conditions took precedence over the potential complications introduced by testing local phenomena on an overall system. The heat and mass transfer coefficients in both phases obtained from this study are discussed in detail in the companion paper (Part II), where comparisons of these results with the limited relevant literature are also presented.

NOMENCLATURE

A	Area (m^2)	C_T	Total molar concentration (kMol/m^3)
Cp	Specific heat (kJ/kg-K)	h	Specific enthalpy (kJ/kg)

LMTD	Log Mean Temperature Difference
M	Molar mass (kg/kMol)
$\dot{m}$	Mass flow rate (kg/s)
$\dot{n}$	Molar flux (kMol/m^2-s)
P	Pressure (kPa)
Q	Heat Duty (kW)
q	Quality
R	Thermal resistance (K/W)
R_R	Resistance ratio
R_W	Wall resistance
T	Temperature (^{o}C)
U	Overall heat transfer coefficient (W/m^2-K)
x	Mass concentration
$\tilde{x}$	Molar concentration
z	Mass concentration of condensing flux
$\tilde{z}$	Molar concentration of condensing flux

Greek Symbols

α	Heat transfer coefficient (W/m^2-K)
β	Mass transfer coefficient (m/s)
$\dot{\Gamma}$	Mass flow rate per unit length per side of tube (kg/m-s)

Subscripts

Abs	Absorber
C	Coolant
fg	Phase change
ID	Inner diameter
in	Inlet
int	Interface
l	Liquid/solution
OD	Outer diameter
out	Outlet
Ref	Refrigerant
T	Total
t	Tube
V	Vapor

ACKNOWLEDGEMENT

The authors would like to acknowledge support for this research from the Air-Conditioning and Refrigeration Technology Institute and the US Department of Energy (ARTI 21CR Program Contract Number 612-10050.)

REFERENCES

Beutler, A., Ziegler, F. and Alefeld, G. (1996), "Falling Film Absorption with Solutions of a Hydroxide Mixture," *International Ab-Sorption Heat Pump Conference*, Montreal, Canada, pp. 303-309.

Bohra, L. K. (2007). "Analysis of Binary Fluid Heat and Mass Transfer in Ammonia-Water Absorption," Ph.D., Mechanical Engineering, Georgia Institute of Technology, Atlanta, GA.

Churchill, S. W. (1977a), "Comprehensive Correlating Equations for Heat, Mass and Momentum Transfer in Fully Developed Flow in Smooth Tubes," *Industrial & Engineering Chemistry, Fundamentals*, **16** (1): 109-116.

Churchill, S. W. (1977b), "Friction-Factor Equation Spans all Fluid-Flow Regimes," *Chemical Engineering Progress*, **84** (24): 91-92.

Colburn, A. P. and Drew, T. B. (1937), "The Condensation of Mixed Vapours," *AIChE Transactions*, **33**: 197-212.

Dorokhov, A. R. and Bochagov, V. N. (1983), "Heat Transfer to a Film Falling over Horizontal Cylinders," *Heat Transfer - Soviet Research*, **15** (2): 96-101.

Fernández-Seara, J., Sieres, J., Rodríguez, C. and Vázquez, M. (2005), "Ammonia-water absorption in vertical tubular absorbers," *International Journal of Thermal Sciences*, **44** (3): 277-288.

Goel, N. and Goswami, D. Y. (2005), "Analysis of a counter-current vapor flow absorber," *International Journal of Heat and Mass Transfer*, **48** (7): 1283-1292.

Gommed, K., Grossman, G. and Koenig, M. S. (2001), "Numerical study of absorption in a laminar falling film of ammonia-water, Atalanta, GA, Amer. Soc. Heating, Ref. Air-Conditoning Eng. Inc., pp. 453-462.

Haselden, G. G. and Malaty, S. A. (1959), "Heat and Mass Transfer Accompanying the Absorption of Ammonia in Water," *Institution of Chemical Engineers -- Transactions*, **37** (3): 137-146.

Hu, X. and Jacobi, A. M. (1996a), "The Inter Tube Falling Film: Part 1- Flow Characteristics, Mode Transition, and Hysteresis," *Journal of Heat Transfer*, **118**: 616-625.

Hu, X. and Jacobi, A. M. (1996b), "The intertube falling film. II. Mode effects on sensible heat transfer to a falling liquid film," *Transactions of the ASME. Journal of Heat Transfer*, **118** (3): 626-33.

Jeong, S., Koo, K.-K. and Lee, S. K. (1998), "Heat transfer performance of a coiled tube absorber with working fluid of ammonia/water," *Proceedings of the 1998 ASHRAE Winter Meeting. Part 2 (of 2), Jan 18-21 1998*, San Francisco, CA, USA, ASHRAE, Atlanta, GA, USA, pp. 1577-1583.

Kang, Y. T., Akisawa, A. and Kashiwagi, T. (1999), "Experimental correlation of combined heat and mass transfer for NH3-H2O falling film absorptionCorrélation expérimentale entre le transfert de chaleur et de masse pour de l'absorption au NH3-H2O à film tombant," *International Journal of Refrigeration*, **22** (4): 250-262.

Killion, J. D. and Garimella, S. (2001), "A critical review of models of coupled heat and mass transfer in falling-film absorption," *International Journal of Refrigeration*, **24** (8): 755-797.

Killion, J. D. and Garimella, S. (2003a), "Gravity-driven flow of liquid films and droplets in horizontal tube banks," *International Journal of Refrigeration*, **26** (5): 516-526.

Killion, J. D. and Garimella, S. (2003b), "A review of experimental investigations of absorption of water vapor in liquid films falling over horizontal tubes," *HVAC and R Research*, **9** (2): 111-136.

Kwon, K. and Jeong, S. (2004), "Effect of vapor flow on the falling-film heat and mass transfer of the ammonia/water absorber," *International Journal of Refrigeration*, **27** (8): 955-964.

Lee, S. (2007). "Development of Techniques for In-Situ Measurement of Heat and Mass Transfer in Ammonia-Water Absorption Systems," Ph.D, Mechanical Engineering, Georgia Institute of Technology, Atlanta, GA.

Nosoko, T., Miyara, A. and Nagata, T. (2002), "Characteristics of falling film flow on completely wetted horizontal tubes and the associated gas absorption," *International Journal of Heat and Mass Transfer*, **45** (13): 2729-2738.

Panchal, C. B., Kuru, W. C., Chen, F. C. and Domingo, N. (1997). Experimental and Analytical Study of Condensation of Ammonia-Water Mixtures. AIChE Symposium Series. **314:** p. 239.

Perez-Blanco, H. (1988), "A Model of an Ammonia-Water Falling Film Absorber," *ASHRAE Transactions*, **94** (1): 467-483.

Potnis, S. V., Anand, G., Gomezplata, A., Erickson, D. C. and Papar, R. A. (1997), "GAX component simulation and validation," *Proceedings of the 1997 ASHRAE Winter Meeting, Jan 26-29 1997*, Philadelphia, PA, USA, ASHRAE, Atlanta, GA, USA, pp. 454-459.

Taylor, B. N. and Kuyatt, C. E. (1994). Guidelines for Evaluating and Expressing the Uncertainty of NIST Measurement Results, National Institute of Standards and Technology.

Wilke, W. (1962), "Heat transfer to falling liquid films (Waermeuebergang an Rieselfilme)," *VDI -- Forschungsheft* (490): 36.